

# Internal Gravity Wave Excitation by Turbulent Convection

D. Lecoanet<sup>1\*</sup> & E. Quataert<sup>1†</sup>

<sup>1</sup>*Astronomy Department and Theoretical Astrophysics Center, University of California, Berkeley, 601 Campbell Hall, Berkeley CA, 94720*

Accepted . Received ; in original form

## ABSTRACT

We calculate the flux of internal gravity waves (IGWs) generated by turbulent convection in stars. We solve for the IGW eigenfunctions analytically near the radiative-convective interface in a local, Boussinesq, and cartesian domain. We consider both discontinuous and smooth transitions between the radiative and convective regions and derive Green’s functions to solve for the IGWs in the radiative region. We find that if the radiative-convective transition is smooth, the IGW flux  $\sim F_{\text{conv}}(d/H)$ , where  $F_{\text{conv}}$  is the flux carried by the convective motions,  $d$  is the width of the transition region, and  $H$  is the pressure scale height. This can be much larger than the standard result in the literature for a discontinuous radiative-convective transition, which gives a wave flux  $\sim F_{\text{conv}}\mathcal{M}$ , where  $\mathcal{M}$  is the convective Mach number. However, in the smooth transition case, the most efficiently excited perturbations will break immediately when they enter the radiative region. The flux of IGWs which do not break and are able to propagate in the radiative region is  $\sim F_{\text{conv}}\mathcal{M}^{5/8}(d/H)^{3/8}$ , larger than the discontinuous transition result by  $(\mathcal{M}H/d)^{-3/8}$ . The transition region in the Sun is smooth for the energy-bearing waves; as a result, we predict that the IGW flux is about five times larger than previous estimates. We discuss the implications of our results for several astrophysical applications, including IGW driven mass loss and the detectability of convectively excited IGWs in main sequence stars.

**Key words:** convection; hydrodynamics; waves; Sun: oscillations

## 1 INTRODUCTION

Internal gravity waves (hereafter, IGWs) are a class of waves in a stably stratified background in which buoyancy serves as a restoring force. IGWs propagate in radiative zones in stars and can influence composition, angular momentum, and energy transport within stars. IGWs could also be important diagnostics of stellar structure—the detection of standing IGWs ( $g$ -modes) has been a long-standing goal of helioseismology (Severny et al. 1976; Brookes et al. 1976), as  $g$ -modes provide better information about the core of the Sun than the more easily observed global sound waves ( $p$ -modes) (e.g., Turck-Chièze et al. 2001). However, IGWs are evanescent in the convection zone, so their surface manifestation is expected to be small.

IGWs have been invoked to explain the observation that F-stars have a smaller than expected Li abundance (e.g., Talon & Charbonnel 1998). Garcia Lopez & Spruit (1991), hereafter GLS91, first suggested that mixing from IGWs could enhance diffusion of Li, leading to lower Li abundances. Charbonnel & Talon (2005) invoke IGWs to explain both the Li abundances of solar-type stars and the rotation of the solar interior. When propagating through a differentially rotating star, selective

damping of modes can deposit the wave’s angular momentum and modify the star’s rotation profile (e.g., Kumar & Quataert 1997; Zahn et al. 1997; Talon et al. 2002). Note, however, that IGWs generally have an anti-diffusive effect, accentuating angular velocity gradients. This anti-diffusive behavior leads to the quasi-biennial oscillation (QBO) in the Earth’s atmosphere, and has been studied extensively by the atmospheric science community (Baldwin et al. 2001; Fritts & Alexander 2003).

Massive stars have convective cores surrounded by a radiative envelope. Quataert & Shiode (2012) suggested that extremely vigorous convection within the last  $\sim$  year of a massive star’s life could generate a super-Eddington IGW flux and drive significant mass loss. Earlier in a massive star’s life, the angular momentum carried by IGWs may generate substantial differential rotation, perhaps mirroring the QBO in the Earth’s atmosphere (Rogers et al. 2012).

In some stars, IGWs are linearly unstable, driven by, e.g., the  $\epsilon$  or  $\kappa$  mechanisms (Unno et al. 1989). Even absent such linear driving, however, IGWs are thought to be generated by turbulent convection. Although IGWs are evanescent in a convective region, they can be excited by Reynolds stresses or entropy fluctuations associated with the convection. A related excitation mechanism is generation by overshooting convective plumes which penetrate into the radiative region. Numerical simulations of a radiative zone adjacent to a convection zone find efficient generation of IGWs (e.g.,

\* E-mail: dlecoanet@berkeley.edu

† E-mail: eliot@berkeley.edu

Rogers & Glatzmaier 2005; Meakin & Arnett 2007; Brun et al. 2011). Although simulations reported in Rogers & Glatzmaier (2005) & Meakin & Arnett (2007) show power distributed over a wide range of frequencies and wavelengths, the power spectra in Brun et al. (2011) exhibit ridges corresponding to discrete  $g$ -modes.<sup>1</sup> Simulations require artificially high diffusivities in the radiative zone to maintain a strong convective flux, and thus IGWs are artificially strongly damped in the radiative zone. This makes it difficult to estimate the IGW flux or quantitatively study the effects of IGWs on the stellar structure.

There have been several efforts to analytically estimate the flux of IGWs stochastically excited by turbulent convection. These models are essential for determining the resulting efficiency of the mixing, angular momentum transport, or mass-loss produced by IGWs. Press (1981, hereafter P81) and GLS91 match pressure perturbations in the convective region to pressure perturbations in the waves, whereas Goldreich & Kumar (1990, hereafter GK90) and B09 calculate eigenmodes and derive how their amplitudes change using an inhomogeneous wave equation. P81, GLS91, and GK90 all model the convective region using mixing length theory, assuming a Kolmogorov turbulence spectrum. B09 uses an energy spectrum calculated from a direct numerical simulation of the solar convection zone. Each of these papers predicts a different IGW power spectrum.

In this paper, we calculate the IGW flux generated by turbulent convection and clarify the relationship between different predictions in the literature. In Section 2, we state our assumptions regarding the background state, and describe some properties of IGWs. Our main calculation is in Section 3, where we introduce our formalism for calculating the IGW flux. Our formalism relies on calculating a Green’s function using the eigenmodes of the system (also discussed in P81). We relate our method to GK90’s in Appendix C. In Section 3.5 we calculate the IGW flux and rms wave displacements for both smooth and discontinuous radiative-convective transitions. Next, we show that our results for a discontinuous transition can be derived more heuristically using pressure balance arguments (Section 4); we also make detailed comparisons to previous results (Section 5). Finally, in Section 6 we conclude, show how our results increase the predicted IGW flux in stars, and discuss some implications of this increased wave flux.

## 2 BACKGROUND STATE AND PERTURBATION EQUATIONS

In this paper we consider a simple model of a radiative zone and adjacent to a convection zone. We assume that the length scales of interest are small in comparison to the stellar radius, i.e., we are in the local limit, so we use cartesian geometry, where  $\mathbf{e}_z$  is the direction of gravity. In our model, the radiative zone is the region  $-L < z < z_i$ , and the convection zone is the region  $z_i < z < L$ , where  $z_i$  is the location of the radiative-convective interface, and both regions have a horizontal area  $\mathcal{A}$ . We take  $L$  and  $\sqrt{\mathcal{A}}$  to be much larger than any other length scale in the problem, and will assume  $z_i$  is close to zero. In Figure 1 we sketch a schematic of

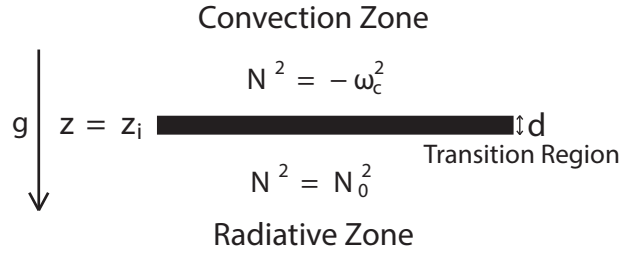


**Figure 1.** A schematic of our problem setup. The radiative-convective interface is at  $z = z_i$ , where  $z_i$  is close to zero, and has width  $d$ . Gravity points downward in the  $z$  direction. The convection zone is the region  $z > z_i$  and the radiative zone is the region  $z < z_i$ . We will use  $\xi_{z,\text{rad}}$  to denote the part of the vertical displacement within the radiative zone. If  $d$  is small, the waves see the radiative-convective transition as discontinuous; we will use superscript  $d$  to denote results for a discontinuous transition. If  $d$  is large, the waves see the radiative-convective transition as smooth; we will use superscript  $s$  to denote results for a smooth transition. Eqns. 41 & 49 give our IGW flux estimates in the discontinuous and smooth limits, respectively.

our model. Using a domain with finite vertical extent provides simpler boundary conditions, but yields the same results as an infinite domain.

Furthermore, we employ the Boussinesq approximation. This is appropriate if the wave generation occurs close to the radiative-convective boundary, and if we are only concerned with IGWs near this boundary. We will see that the wave generation primarily occurs in a region with height approximately equal to the size of the energy bearing convective motions, which we assume is  $\sim H$  the pressure scale height. Although the Boussinesq approximation is only rigorously valid on length scales smaller than  $H$ , we recover results similar to those presented in GK90 who used the fully compressible equations. We thus believe that our results would not change qualitatively if we used the fully compressible equations.

We model the radiative region as a stably stratified atmosphere with a squared buoyancy frequency  $N_0^2$ . The convective region is much more complicated due to turbulent motions. We decompose the fluid properties in the convection zone into time averaged and fluctuating components. We assume the time averaged velocity is zero, and there is a very small mean stratification with squared buoyancy frequency  $-\omega_c^2$ . Because the convective region is nearly adiabatic,  $\omega_c \ll N_0$ . We treat the fluctuating components of the velocity and entropy in the convective region as source terms in the wave equation. In practice, we only include source terms due to the Reynolds stress in our analysis; source terms due to entropy fluctuations are of the same size or smaller than the Reynolds stress terms (P81, GK90).

With these assumptions, the equation for the evolution of the vertical displacement  $\xi_z$  is

$$\nabla^2 \frac{\partial^2}{\partial t^2} \xi_z + N_0^2 \nabla_{\perp}^2 \xi_z = 0, \quad (1)$$

in the radiative region, and

$$\nabla^2 \frac{\partial^2}{\partial t^2} \xi_z - \omega_c^2 \nabla_{\perp}^2 \xi_z = S = -\nabla^2 F_z + \frac{\partial}{\partial z} \nabla_{\perp} \cdot \mathbf{F}, \quad (2)$$

in the convective region. We take  $\nabla_{\perp} = \partial_x \mathbf{e}_x + \partial_y \mathbf{e}_y$  to be the horizontal part of the gradient operator (perpendicular to gravity), and  $S$  to be the source term due to the Reynolds stress  $\mathbf{F} = \nabla \cdot (\mathbf{u}_c \mathbf{u}_c)$  associated with convective motions  $\mathbf{u}_c$ .

We now discuss the wave solutions to the homogeneous equations, i.e., taking  $S = 0$ . Because the equations are autonomous in

<sup>1</sup> The simulations of Rogers & Glatzmaier (2005) and Brun et al. (2011) solve the anelastic equations, which do not conserve energy (Brown et al. 2012). This could potentially produce errors in the IGW amplitudes and/or power spectra.

$x, y, t$ , we can Fourier transform in these directions. Thus, we can take the solutions to be

$$\xi_z(x, y, z, t) = \xi_z(z) \exp(ik_x x + ik_y y - i\omega t), \quad (3)$$

and define the horizontal wavenumber  $k_\perp = \sqrt{k_x^2 + k_y^2}$ , i.e., the wavenumber perpendicular to gravity. Throughout this paper we will assume  $N_0 \gg \omega$ . The solutions to eqns. 1,2 are

$$\xi_z = B_1 \cos(N_0 k_\perp z / \omega) + B_2 \sin(N_0 k_\perp z / \omega), \quad (4)$$

$$\xi_z = C_1 \exp(-k_\perp z) + C_2 \exp(k_\perp z), \quad (5)$$

respectively, where we have assumed  $\sqrt{\omega^2 + \omega_c^2} \sim \omega$ . The horizontal displacement  $\xi_\perp$  and pressure perturbation  $\delta p$  are related to  $\xi_z$  by

$$\xi_\perp \sim i(N_0/\omega)\xi_z, \quad (6)$$

$$\delta p \sim i\rho_0(N_0\omega/k_\perp)\xi_z, \quad (7)$$

in the radiative region, and

$$\xi_\perp \sim \xi_z, \quad (8)$$

$$\delta p \sim \rho_0(\omega^2/k_\perp)\xi_z, \quad (9)$$

in the convective region. The background density is  $\rho_0$ , which is constant to lowest order in the Boussinesq approximation.

To solve for the coefficients in eqns. 4 & 5 and the eigenvalues  $\omega$ , we must impose four boundary conditions and a normalization condition (the latter is discussed in Section 3.3). Two of the boundary conditions are on the behavior of  $\xi_z$  at  $z = \pm L$ . The physical solution requires that  $\xi_z = 0$  at the top and bottom boundaries. The other two boundary conditions are set at the radiative-convective interface,  $z = z_i$ . These depend on the nature of the boundary between the radiative and convective regions, and determine which  $\omega$  satisfy the eigenvalue problem. Assume that  $N^2$  varies from  $N_0^2$  to  $-\omega_c^2$  in a thin layer with height  $d$ , as illustrated in Figure 1. If there is a sharp transition between the radiative and convective regions, i.e.,  $(k_\perp N_0/\omega)d \ll 1$ , we can make the approximation that  $N^2$  is discontinuous at  $z_i$ , which we take to be at  $z = 0$ . However, if  $N^2$  varies slowly, i.e.,  $(k_\perp N_0/\omega)d \gg 1$ , then interesting behavior can take place in the transition region. As we discuss in Section 6, we expect the most efficiently excited waves in the Sun to fall under this latter regime. We will discuss both the discontinuous and smooth  $N^2$  limits below.

### 3 WAVE GENERATION BY TURBULENT CONVECTION

Because the wave generation and wave propagation regions are distinct, we use a Green's function (or equivalently, variation of parameters), as in P81. Once we have a Green's function  $G(z, t; \zeta, \tau)$ , we can write the vertical displacement in the radiative region as

$$\xi_{z,\text{rad}} = \int_{-\infty}^t d\tau \int_{z_i}^L d\zeta G(z, t; \zeta, \tau) S(x, y, \zeta, \tau), \quad (10)$$

where we assume that  $\xi_{z,\text{rad}}$  is zero at  $t \rightarrow -\infty$ . The Green's function depends on whether  $N^2$  can be modeled as discontinuous or smooth at the radiative-convective boundary. In Section 3.1 we calculate the Green's function assuming  $N^2$  is discontinuous (as was assumed in GLS91 and GK90) and then in Section 3.2 we treat the smooth  $N^2$  case. As we shall argue, the latter is more appropriate for the low frequency waves which dominate the IGW flux. In Appendix C we show that the Green's function method is formally equivalent to GK90's method of expanding  $\xi_z$  into normal modes to solve eqns. 1, 2.

#### 3.1 Green's Function for Discontinuous $N^2$

To calculate the Green's function, we need two linearly independent solutions, one which satisfies  $\xi_z(-L) = 0$ , and one that satisfies  $\xi_z(+L) = 0$ . The boundary conditions at  $z_i$ , which we take to be at  $z = 0$ , when  $N^2$  is discontinuous, are that  $\xi_z$  and  $\delta p$  are continuous at  $z = 0$ . The first solution, which we call  $\eta_z^d$ , satisfies the boundary condition at  $z = +L$ :

$$\eta_z^d = \begin{cases} B_1 \cos(N_0 k_\perp z / \omega + \omega / N_0) & z < 0, \\ B_1 \exp(-k_\perp z) & z > 0. \end{cases} \quad (11)$$

Here we use *superscript d* to denote the eigenfunction when  $N^2$  is *discontinuous* at the interface. In Section 3.2 we will use *superscript s* to denote quantities when  $N^2$  is *smooth* at  $z = 0$ . The second linearly independent solution, which we call  $\xi_z^d$ , satisfies the boundary condition at  $z = -L$ :

$$\xi_z^d = \begin{cases} B_2 \sin(N_0 k_\perp z / \omega) & z < 0, \\ B_2 \frac{N_0}{2\omega} (\exp(k_\perp z) - \exp(-k_\perp z)) & z > 0. \end{cases} \quad (12)$$

The eigenvalues  $\omega$  must satisfy  $\sin(N_0 k_\perp L / \omega) = 0$ . Later we will project the total vertical displacement in the radiative zone onto the basis  $\{\xi_z\}_\omega$ . The vertical displacement in the radiative zone is approximately orthogonal to  $\{\eta_z\}_\omega$  in the radiative zone. Thus, it is important that our second linearly independent solution is also approximately orthogonal to  $\{\eta_z\}_\omega$ , as is the case for eqns. 11 & 12.

The general expression for the Green's function, assuming  $z < \zeta$ , is

$$G(z, t; \zeta, \tau) = \int d\omega' \frac{\delta(f(\omega'))}{\omega'^2} \frac{\xi_z(z; \omega') \eta_z(\zeta; \omega')}{W(\zeta)} \exp(-i\omega'(t - \tau)), \quad (13)$$

where we label the eigenfunctions with their frequency  $\omega'$ ,  $\delta$  denotes the Dirac delta function, and  $W(\zeta)$  denotes the Wronskian of  $\xi_z$  and  $\eta_z$ .  $f(\omega')$  is a function which is zero if and only if  $\omega'$  is an eigenvalue. For the discontinuous case, we have  $f(\omega') = \sin(N_0 k_\perp L / \omega')$ . We thus can simplify eqn. 13 to

$$G(z, t; \zeta, \tau) = \sum_{\omega'} \frac{1}{N_0 k_\perp L} \frac{\xi_z(z; \omega') \eta_z(\zeta; \omega')}{W(\zeta)} \exp(-i\omega'(t - \tau)), \quad (14)$$

where the sum is over the eigenvalues  $\omega'$ . For the discontinuous  $N^2$  problem, assuming  $z < 0$  and  $\zeta > 0$ , the Green's function is

$$G^d(z, t; \zeta, \tau) = \sum_{\omega'} \frac{\omega'}{N_0^2 k_\perp^2 L} \frac{1}{B_2} \xi_z^d(z; \omega') \exp(-k_\perp \zeta - i\omega'(t - \tau)). \quad (15)$$

#### 3.2 Green's Function for Smooth $N^2$

If  $N^2$  varies smoothly from  $N_0^2$  to  $-\omega_c^2$ , then a WKB type approximation can be used, provided that  $N_0 k_\perp d / \omega \gg 1$ . Our motivation for studying this limit is that the largest scale eddies in stars satisfy  $N_0 k_\perp d / \omega \gg 1$  (see Section 6). We would like to develop an approximate solution which is valid within the transition region, allowing us to connect the solution in the radiative region (eqn. 4) to the solution in the convective region (eqn. 5).

The solution in the transition region depends on the form of  $N^2(z)$  near the radiative-convective interface. In Appendix B, we consider a piecewise linear  $N^2$  profile. This is the most abrupt continuous transition possible. We find that the Green's function for a piecewise linear  $N^2$  is larger by a factor of  $(N_0 k_\perp d / \omega)^{1/6}$  than the Green's function for discontinuous  $N^2$ , implying that wave excitation is more efficient by a factor of  $(N_0 k_\perp d / \omega)^{1/3}$ .

Here we will consider the case of a tanh profile. We believe

a tanh profile is a good approximation to  $N^2$  near the radiative-convective interface. An eigenmode with frequency  $\omega$  transitions from oscillatory behavior to exponential behavior at a point  $z_t$  (where  $N^2 = \omega^2$ ), which is lower than the radiative-convective interface,  $z_i$  (where  $N^2 = 0$ ). For a tanh profile,  $z_t$  does not change very much as  $\omega$  changes; although it is smooth, it is not *too* smooth.

One might be tempted to appeal to WKB analysis to solve for the eigenfunction on either side of the interface, and then match across the interface by expanding  $N^2$  to linear order near the wave's turning point (as is standard in, e.g., quantum mechanics). Roughly, a WKB solution is valid if the local wavelength of the eigenfunction is small compared to the scale on which the wavenumber of the eigenfunction varies, which for us is  $d$ . For smooth  $N^2$  we have assumed  $N_0 k_\perp d / \omega \gg 1$ , so the WKB solution in the radiative zone is valid. However, the WKB solution might break down near the convection zone if  $k_\perp d \ll 1$ . Indeed, for the tanh profile, the eigenfunction is poorly approximated by the WKB solution when  $k_\perp d \ll 1$ . Moreover, because  $d/H \leq 1$  and IGWs with  $k_\perp H \sim 1$  dominate the wave flux (see Section 3.5;  $H$  here is the pressure scale height which we assume is the largest scale of the turbulence), the WKB solution fails for the most efficiently excited IGWs. Instead, we need to develop a different method to solve for the eigenfunctions. The details of this calculation are given in Appendix A.

We assume  $N^2(z)$  is given by

$$N^2(z) = \frac{N_0^2 + \omega_c^2}{2} \left( \tanh\left(-\frac{z}{d}\right) + 1 \right) - \omega_c^2. \quad (16)$$

In Appendix A, we derive approximate forms for two independent eigenfunctions, and show that there is excellent agreement between the numerical solutions to the eigenvalue problem and our asymptotic Bessel function solutions. We are interested in the behavior of the eigenfunctions near the radiative-convective interface  $z_i$ . The interface is at

$$\exp\left(-2\frac{z_i}{d}\right) \sim \frac{\omega_c^2}{N_0^2 + \omega_c^2}. \quad (17)$$

The two independent solutions are

$$\eta_z^s \sim \begin{cases} B_1 \cos(N_0 k_\perp z / \omega + \pi/4) & z \gtrsim -d \\ B_1 \left(\frac{N_0 k_\perp d}{\omega}\right)^{1/2} \left(\frac{\omega}{\bar{\omega}}\right)^{k_\perp d} J_{\bar{d}} \left[\frac{\omega k_\perp d}{\bar{\omega}} \exp\left(-\frac{z-z_i}{d}\right)\right] & z \lesssim d \end{cases} \quad (18)$$

$$\xi_z^s \sim \begin{cases} B_2 \sin(N_0 k_\perp z / \omega + \pi/4) & z \gtrsim -d \\ B_2 \left(\frac{N_0 k_\perp d}{\omega}\right)^{1/2} \left(\frac{\bar{\omega}}{\omega}\right)^{k_\perp d} Y_{\bar{d}} \left[\frac{\omega k_\perp d}{\bar{\omega}} \exp\left(-\frac{z-z_i}{d}\right)\right] & z \lesssim d \end{cases} \quad (19)$$

where  $\bar{\omega}^2 = \omega_c^2 + \omega^2$  and  $\bar{\omega}/\omega$  ranges between  $\sqrt{2}$  and 1 for  $\omega \gtrsim \omega_c$ , and  $\bar{d} = \bar{\omega} k_\perp d / \omega$ . In eqns. 18 & 19 we have dropped several factors of order unity from the equations derived in Appendix A. The eigenvalues for this problem are the frequencies  $\omega$  which satisfy  $\sin(-N_0 k_\perp L / \omega + \pi/4) = 0$ .

Given eqns. 18 & 19, the Green's function, for  $z < 0$  and  $\zeta > 0$  is

$$G^s(z, t; \zeta, \tau) \sim \sum_{\omega'} \left(\frac{\omega' d}{N_0 k_\perp}\right)^{1/2} \left(\frac{\omega'}{\bar{\omega}}\right)^{k_\perp d} (B_2 N_0 k_\perp L)^{-1} \times J \xi_z^s(z; \omega') \exp(-k_\perp \zeta - i\omega'(t - \tau)), \quad (20)$$

where we introduce the shorthand

$$J \equiv J_{\bar{d}} \left(\frac{\omega k_\perp d}{\bar{\omega}}\right). \quad (21)$$

Using series expansions from Abramowitz & Stegun (1972), we can approximate

$$J \sim \begin{cases} 1 & \text{if } k_\perp d \ll 1, \\ (k_\perp d)^{-1/2} \exp(-k_\perp d) & \text{if } k_\perp d \gg 1. \end{cases} \quad (22)$$

Note that although the smooth and discontinuous Green's functions are equal to one another when  $N_0 k_\perp d / \omega \sim 1$ , the Green's function in eqn. 20 is no longer valid when  $N_0 k_\perp d / \omega \ll 1$  (see Appendix A1). Instead, eqn. 15 must be used in this limit.

### 3.3 Amplitude Equation

Now that we have the Green's function, we can calculate mode excitation. First, we will expand  $\xi_{z,\text{rad}}$  (in eqn. 10) into eigenmodes  $\xi_{z,\text{rad}}(z; \omega)$ . We use the subscript rad to denote the  $z < z_i$  part of the eigenfunctions (eqns. 12, 19). We write

$$\xi_{z,\text{rad}} = \frac{1}{\sqrt{\mathcal{A}}} \sum_{\omega'} A(t; \omega') \xi_{z,\text{rad}}(z; \omega') \exp(ik_x x + ik_y y - i\omega' t), \quad (23)$$

where the  $\xi_{z,\text{rad}}$  are the  $z < z_i$  part of the eigenmodes. Using this representation in eqn. 10, we take the inner product with  $\xi_{z,\text{rad}}(z; \omega)$ , multiply by  $\exp(-ik_x x - ik_y y + i\omega t)$ , and integrate over  $dxdy$  to find

$$A(t; \omega) = \frac{1}{\sqrt{\mathcal{A}}} \int_{-\infty}^t d\tau \int dxdy \int_{z_i}^L d\zeta \frac{1}{N_0 k_\perp L} \frac{\eta_z(\zeta; \omega)}{W(\zeta)} \times S(x, y, \zeta, \tau) \exp(-ik_x x - ik_y y + i\omega \tau). \quad (24)$$

This procedure is discussed more thoroughly in Appendix C.

At this point we must pick a normalization condition for our eigenfunctions. The energy in the perturbation is

$$\int d^3 x \rho_0 \left| \frac{\partial}{\partial t} \xi_{\text{rad}}(z) \right|^2 = \sum_{\omega} \sum_{\omega'} A(\omega) A^*(\omega') \left( \omega \omega' \int dz \rho_0 \xi_{\text{rad}}(z, \omega) \cdot \xi_{\text{rad}}^*(z, \omega') \right) \quad (25)$$

We want to identify  $\sum_{\omega} |A(\omega)|^2$  with the energy, so our normalization condition is

$$\omega \omega' \int dz \rho_0 \xi_{\text{rad}}(z; \omega) \cdot \xi_{\text{rad}}^*(z; \omega') = \delta_{\omega \omega'}, \quad (26)$$

where  $\delta$  is the Kronecker delta. Using the eigenfunctions (eqns. 11, 12, 18, 19) and the polarization relation (eqn. 6), the normalization condition implies

$$B^2 \sim B_1^2 \sim B_2^2 \sim \frac{1}{N_0^2 L \rho_0}, \quad (27)$$

for both smooth and discontinuous  $N^2$ . Using this normalization in eqn. 24, the amplitude equations are

$$A^d(t; \omega) = \frac{1}{\sqrt{\mathcal{A}}} \int_{-\infty}^t d\tau \int dxdy \exp(-ik_x x - ik_y y + i\omega \tau) \times \frac{\omega}{N_0 k_\perp^2} \sqrt{\frac{\rho_0}{L}} \int_{z_i}^L d\zeta \exp(-k_\perp \zeta) S(x, y, \zeta, \tau), \quad (28)$$

$$A^s(t; \omega) = \frac{1}{\sqrt{\mathcal{A}}} \int_{-\infty}^t d\tau \int dxdy \exp(-ik_x x - ik_y y + i\omega \tau) \times \left( \frac{J \sqrt{\omega N_0 \rho_0 d}}{\sqrt{L k_\perp^3}} \right) \left(\frac{\omega}{\bar{\omega}}\right)^{k_\perp d} \int_{z_i}^L d\zeta \exp(-k_\perp \zeta) S(x, y, \zeta, \tau). \quad (29)$$

### 3.4 Model of Turbulent Convection

To make further progress, we need to specify the source term  $S$ . We assume that the convective turbulence is comprised of a large number of incoherent eddies, estimate the wave generation due to a single eddy in isolation, and then find the total wave generation by summing over all eddies. We model the statistical properties of stellar convection using Kolmogorov turbulence (see, e.g.,

Goldreich & Keeley 1977): the convective velocity on the outer-scale  $H$  is  $u_c$  and the associated convective turnover frequency is  $\omega_c \sim u_c/H$ . The convective energy flux is  $F_{\text{conv}} \sim \rho_0 u_c^3$ . On scales  $h$  sufficiently small compared to  $H$ , the turbulent power-spectrum is given by the Kolmogorov scaling:

$$u_h \simeq u_c (h/H)^{1/3} \simeq u_c (\omega_e/\omega_c)^{-1/2} \quad (30)$$

where we have used the fact that smaller eddies have higher frequencies, i.e., shorter turnover times, with  $\omega_e \simeq u_h/h \propto h^{-2/3}$  and thus  $h \propto \omega_e^{-3/2}$ . A given convective eddy characterized by its frequency  $\omega_e$  can excite waves having frequencies  $\omega$  and horizontal wavenumbers  $k_\perp$  that satisfy

$$\omega \lesssim \omega_e \quad \text{and} \quad k_\perp \lesssim k_\perp^{\text{max}} \simeq H^{-1}(\omega_e/\omega_c)^{3/2}. \quad (31)$$

### 3.5 Energy Generation Rates and IGW Fluxes

We can now estimate the energy generation due to a single eddy with size  $h$  and turnover frequency  $\omega_e$ . The source term contains three spatial derivatives which we can integrate by parts. The contribution due to the source term is

$$S \sim k_\perp^3 u_h^2. \quad (32)$$

Assuming the eddy has volume  $h^3$  and lasts for a time  $\omega_e^{-1}$ , we can estimate the change in the amplitude due to a single eddy

$$\Delta A^d(\omega) \sim \sqrt{\frac{\rho_0}{\mathcal{A}L} \frac{\omega}{N_0}} k_\perp h^4 u_h, \quad (33)$$

$$\Delta A^s(\omega) \sim \sqrt{\frac{N_0}{\omega}} (J \sqrt{k_\perp d}) \left(\frac{\omega}{\bar{\omega}}\right)^{k_\perp d} \Delta A^d(\omega). \quad (34)$$

The total energy generation rate due to all eddies is then

$$\dot{E}^d(\omega) \sim \frac{(\Delta A^d)^2}{\omega_e^{-1}} \left(\frac{\mathcal{A}k_\perp^{-1}}{h^3}\right) \sim \frac{\rho_0}{L} \left(\frac{\omega}{N_0}\right)^2 u_h^3 h^3 (k_\perp h), \quad (35)$$

$$\dot{E}^s(\omega) \sim \frac{N_0}{\omega} (J \sqrt{k_\perp d})^2 \left(\frac{\omega}{\bar{\omega}}\right)^{2k_\perp d} \dot{E}^d(\omega). \quad (36)$$

The factor of  $\mathcal{A}k_\perp^{-1}/h^3$  in eqn. 35 counts the number of eddies with size  $h$  which excite IGWs with frequency  $\omega$ . We have assumed excitation happens in a region with thickness  $dz \sim k_\perp^{-1}$  (because the IGW eigenfunction decreases in the convection zone over a characteristic lengthscale  $\sim k_\perp^{-1}$ ). Because of the random phases of the convective eddies, the excitations due to different eddies are assumed to be uncorrelated, and the energy increases only linearly with the number of eddies.

The IGW flux is given by

$$\begin{aligned} \frac{dF^d}{d \log \omega d \log k_\perp} &\sim \frac{\dot{E}^d(\omega)}{\mathcal{A}} \left(\mathcal{A}k_\perp^2 Lk_\perp \frac{N_0}{\omega}\right) \\ &\sim \rho_0 u_h^3 \frac{\omega}{N_0} (k_\perp h)^4 \sim \rho_0 u_c^3 \mathcal{M} (k_\perp H)^4 \left(\frac{\omega}{\omega_c}\right)^{-13/2}, \end{aligned} \quad (37)$$

$$\frac{dF^s}{d \log \omega d \log k_\perp} \sim \rho_0 u_c^3 (k_\perp H)^4 \left(\frac{\omega}{\omega_c}\right)^{-15/2} (J^2 k_\perp d) \left(\frac{\omega}{\bar{\omega}}\right)^{2k_\perp d} \quad (38)$$

where  $\mathcal{M} = \omega_c/N_0$  is the convective Mach number. The term in parentheses in the first equality of eqn. 37 is the density of states. There are  $\mathcal{A}k_\perp^2$  modes in the horizontal direction, and  $Lk_\perp N_0/\omega$  modes in the vertical direction, with wavenumber  $\sim k_\perp$  and frequency  $\sim \omega$ , which each contribute a flux  $\dot{E}(\omega)/\mathcal{A}$ . Recall that eqns. 37, 38 only apply for  $\omega \gtrsim \omega_c$  and  $k_\perp \lesssim k_\perp^{\text{max}}(\omega) \sim H^{-1}(\omega/\omega_c)^{3/2}$ .

Now consider how the flux varies with  $k_\perp$ . In the case of

smooth  $N^2$ , the flux decreases exponentially for  $k_\perp d \gg 1$  because of the  $J^2$  term in eqn. 38 (see eqn. 22). The dominant contribution to the flux is from  $k_\perp d \lesssim 1$ , so for the rest of this section, we will assume  $k_\perp d \lesssim 1$ , and thus  $J \sim 1$ . Assuming that  $d/H < 1$ , and integrating over  $k_\perp$ , we find

$$\frac{dF^d}{d \log \omega} \sim \rho_0 u_c^3 \mathcal{M} \left(\frac{\omega}{\omega_c}\right)^{-1/2}, \quad (39)$$

$$\frac{dF^s}{d \log \omega} \sim \begin{cases} \rho_0 u_c^3 \left(\frac{d}{H}\right) & \omega \lesssim \omega_c (H/d)^{2/3}, \\ \rho_0 u_c^3 \left(\frac{\omega}{\omega_c}\right)^{-15/2} \left(\frac{H}{d}\right)^4 & \omega \gtrsim \omega_c (H/d)^{2/3}. \end{cases} \quad (40)$$

Finally, we find that the total flux is

$$F^d \sim \rho_0 u_c^3 \mathcal{M} \sim F_{\text{conv}} \mathcal{M}, \quad (41)$$

$$F^s \sim \rho_0 u_c^3 \left(\frac{d}{H}\right) \sim F_{\text{conv}} \left(\frac{d}{H}\right). \quad (42)$$

This estimate predicts, for a smooth  $N^2$  profile, an IGW flux only slightly smaller than the convective flux. However, as we now show, energy-bearing waves in the smooth  $N^2$  case will undergo vigorous wave-breaking as soon as they enter the radiative zone, and thus cannot be considered waves. Instead, these large scale waves can be thought of a manifestation of penetrative convection in this calculation.

To quantify this argument, we calculate the typical size of the perturbations in the radiative zone using

$$\frac{dF}{d \log \omega d \log k_\perp} \sim \rho_0 (\omega \xi_\perp)^2 u_{g,z}, \quad (43)$$

where  $u_{g,z} \sim \omega/k_z \sim \omega^2/(N_0 k_\perp)$  is the vertical group velocity, and we have assumed  $\xi_\perp \gg \xi_z$  (eqn. 6). From this, we find

$$\xi_z^d \sim H \frac{\omega}{N_0} (k_\perp H)^{5/2} \left(\frac{\omega}{\omega_c}\right)^{-21/4}, \quad (44)$$

$$\xi_z^s \sim H \sqrt{\frac{\omega}{N_0}} (k_\perp H)^3 \left(\frac{\omega}{\omega_c}\right)^{-21/4} \left(\frac{d}{H}\right)^{1/2} \left(\frac{\omega}{\bar{\omega}}\right)^{k_\perp d} \quad (45)$$

and

$$k_z \xi_z^d \sim (k_\perp H)^{7/2} \left(\frac{\omega}{\omega_c}\right)^{-21/4}, \quad (46)$$

$$k_z \xi_z^s \sim \mathcal{M}^{-1/2} (k_\perp H)^4 \left(\frac{\omega}{\omega_c}\right)^{-23/4} \left(\frac{d}{H}\right)^{1/2} \left(\frac{\omega}{\bar{\omega}}\right)^{k_\perp d}. \quad (47)$$

Recall that the condition for wave breaking is  $k_z \xi_z \sim 1$ . For the case of discontinuous  $N^2$ , the most efficiently excited waves are marginally susceptible to wave breaking. However, for the case of smooth  $N^2$ , the most efficiently excited waves will immediately break once they enter the radiative region. Thus, these perturbations are not actually waves, as they do not stay coherent.

The only waves that successfully propagate in the radiative zone have  $k_z \xi_z \lesssim 1$ . Thus, to find the IGW flux for smooth  $N^2$ , we must integrate the flux only over the regions of  $(k_\perp, \omega)$  space in which  $k_z \xi_z \lesssim 1$ . This implies

$$(HM/d)^{1/2} \lesssim (k_\perp H)^4 \left(\frac{\omega}{\omega_c}\right)^{-23/4}, \quad (48)$$

and, as before,  $\omega \gtrsim \omega_c$ ,  $k_\perp \lesssim H^{-1}(\omega/\omega_c)^{3/2}$ , and  $k_\perp d \lesssim 1$ . We find that the waves that are marginally susceptible to wave breaking, and which maximize the flux are at the convective turnover frequency,  $\omega \sim \omega_c$ , but have small wave numbers,  $k_\perp H \sim (MH/d)^{1/8}$ . For these waves,

$$F^s \sim F_{\text{conv}} \mathcal{M}^{5/8} \left(\frac{d}{H}\right)^{3/8}. \quad (49)$$

This result is only valid if these waves see a smooth  $N^2$  profile, i.e.,

$$(MH/d)^{-7/8} \gg 1. \quad (50)$$

If this condition is satisfied, then the IGW flux is larger than that predicted by the discontinuous result by  $(MH/d)^{-3/8}$ . Note that if  $d/H \sim \mathcal{M}$ , then the discontinuous and smooth  $N^2$  limits give the same wave flux.

#### 4 PRESSURE PERTURBATION BALANCE

A more heuristic way to derive the IGW flux is to compare the pressure perturbation on either side of the radiative-convective boundary. This argument is not sufficiently precise to treat the smooth  $N^2$  case—hence, we will assume  $N^2$  is discontinuous, and thus that the pressure perturbation is continuous at the radiative-convective interface at  $z = 0$ . The pressure perturbation associated with a convective eddy with a turnover frequency  $\omega_e$  and size  $h$  is

$$\delta p_{\text{conv}} \sim \rho_0 v_h^2 \sim \rho_0 u_c^2 (\omega_e/\omega_c)^{-1}. \quad (51)$$

The polarization condition (eqn. 7) relates the pressure perturbation in the radiative zone to the vertical displacement,

$$\delta p_{\text{rad}} \sim \rho_0 \frac{N_0 \omega \xi_z}{k_\perp}. \quad (52)$$

We assume the convective eddy can only effectively couple to an IGW if the frequencies and horizontal wavelengths match, which requires  $\omega_e \sim \omega$  and  $k_\perp \sim h^{-1}$ .

A large number of convective eddies contribute to driving a given standing IGW. This is particularly true for  $k_\perp H \gg 1$  and/or  $\omega \gg \omega_c$  because then small eddies with sizes  $h \ll H$  are responsible for the driving. The number of eddies contributing to the excitation of a given standing wave is

$$\mathcal{N} \sim \frac{\mathcal{A} dz}{h^3} \sim (\mathcal{A} h^{-2}) (k_\perp H)^{-1} \left( \frac{\omega}{\omega_c} \right)^{9/2} \quad (53)$$

where we have assumed  $\omega \gtrsim \omega_c$  and that the excitation happens in a region with thickness  $dz \sim k_\perp^{-1}$  (see also eqn. 35). Because an individual IGW is excited by many uncorrelated eddies, the effective pressure fluctuation driving a wave is reduced by a factor of  $\sqrt{\mathcal{N}}$  relative to that given in eqn. 51.

When  $N^2$  is discontinuous at  $z = 0$  one of the boundary conditions is that  $\delta p$  is continuous at  $z = 0$ , so that  $\delta p_{\text{rad}} \sim \delta p_{\text{conv}}$ . Using eqns. 51–53, we find that the amplitude of a mode with frequency  $\sim \omega$  and wavenumber  $\sim k_\perp$  is

$$\xi_z^d \sim \frac{\delta p_{\text{conv}} k_\perp}{\rho_0 N_0 \omega \sqrt{\mathcal{N}}} \sim H^2 k_\perp \frac{\omega_c^3}{N_0 \omega^2} \mathcal{N}^{-1/2}. \quad (54)$$

However, there are  $\mathcal{A} k_\perp^2$  such modes in the domain (we have already implicitly summed over the vertical modes in deriving eqns. 51, 52), so the typical rms vertical displacement is

$$\xi_z^d \sim H^2 k_\perp \frac{\omega_c^3}{N_0 \omega^2} \sqrt{\frac{\mathcal{A} k_\perp^2}{\mathcal{N}}} \sim H \frac{\omega}{N_0} (k_\perp H)^{5/2} \left( \frac{\omega}{\omega_c} \right)^{-21/4}, \quad (55)$$

the same result as in the inhomogeneous wave equation calculation (eqn. 44).

#### 5 COMPARISON WITH PREVIOUS WORK

In this section, we discuss the relationship between our results and previous calculations in the literature. We begin with GK90, who

only consider the discontinuous  $N^2$  case. GK90 solved the fully compressible inhomogeneous wave equation by expanding the perturbation in terms of normal modes and then deriving an amplitude equation. This is equivalent to our Green's function method (see Appendix C). Their end result is very similar to our own; for  $k_\perp H \ll 1$  they find

$$\frac{dF}{d \log \omega d \log k_\perp} \sim \mathcal{M} \rho_0 u_c^3 (k_\perp H)^3 \left( \frac{\omega}{\omega_c} \right)^{-13/2} \quad (\text{GK90; eq. 73}) \quad (56)$$

This differs from our result (eqn. 37) by a factor of  $k_\perp H^2$ . We arrive at a different IGW flux because in the Boussinesq approximation  $\partial_z \xi_z \sim k_\perp \xi_z$ , whereas for the fully compressible system,  $\partial_z \xi_z \sim \xi_z/H$  when  $k_\perp H \ll 1$ . Accounting for both  $k_\perp H \gtrsim 1$  and  $k_\perp H \lesssim 1$ , the correct scaling of the IGW flux with  $k_\perp H$  is  $F \sim (k_\perp H)^3 (1 + k_\perp H)$ . Taking this into account in our smooth  $N^2$  calculation, the flux of IGWs which do not break changes to  $F^d \sim F_{\text{conv}} \mathcal{M}^{15/23} (d/H)^{8/23}$ , which is very close to the flux in eqn. 49.

Because GK90 solve the fully compressible equations, they include multiple scale heights in their convection zone. They find that the most efficient excitation of waves with frequency  $\omega$  is at the height where the turnover frequency of the energy bearing eddies is about equal to  $\omega$ . This effect would be straightforward to include in our model—one would need to derive a Green's function based on the fully compressible eigenfunctions, and then convolve with a vertically varying source term.

GLS91 use a pressure balance argument to study the discontinuous  $N^2$  case. Their power spectrum agrees with eqn. 37 when  $\omega \sim \omega_c$  and  $k_\perp H \sim 1$ , but not at higher frequencies or wave numbers. They assume that the pressure perturbation in the convection zone equals the pressure perturbation in the radiative zone. They take  $\delta p_{\text{conv}} \sim \rho_0 u_h^2$ , and  $\delta p_{\text{rad}} \sim \rho_0 (\omega \xi_\perp)^2$ . This expression for the pressure perturbation in the radiative zone does not satisfy the polarization condition  $\delta p_{\text{rad}} \sim \rho_0 (N_0 \omega/k_\perp) \xi_z$  (eqn. 7), unless  $\xi_\perp \sim k_\perp^{-1}$ . Because many eddies contribute to the excitation of a single IGW mode, GLS91 also decrease their IGW amplitude by a factor of  $1/\sqrt{\mathcal{N}}$ . However, they only account for the incoherent sum of small eddies at the interface producing perturbations on large spatial scales. This gives  $\mathcal{N}_{\text{GLS91}} \sim (k_\perp h)^{-2}$ , where  $k_\perp h \ll 1$ . In our analysis, we include eddies which are a distance  $k_\perp^{-1}$  above the interface, and we take into account that IGWs excited in different parts of the domain incoherently interfere with each other as they propagate in the radiative zone. These additional effects yield  $\mathcal{N} \sim \mathcal{A} k_\perp^{-1}/h^3$ .

P81 uses two different techniques to calculate the IGW flux. The first uses a pressure balance argument. Press uses that  $\delta p_{\text{conv}} \sim \rho_0 u_h^2$ , and that  $\delta p_{\text{rad}} \sim (\rho_0 N_0 \omega/k_\perp) \xi_z$ , and that these pressure perturbations are about equal at the interface. Throughout his analysis, Press assumes  $k_\perp^{-1} \sim h$ . Thus, Press finds

$$\xi_z \sim \frac{(k_\perp h)^2}{k_z} \sim \frac{1}{k_z}, \quad (\text{P81; eq. 75}) \quad (57)$$

This is the same result given by GLS91, and is consistent with our own assuming  $k_\perp h \sim 1$ . This is because  $\mathcal{A} k_\perp^2/\mathcal{N} \sim 1$  when  $k_\perp h \sim 1$ .

<sup>2</sup> Although our final results are similar, there are some ambiguities in GK90's derivation. In deriving their eqn. 48 from their eqn. 45, GK90 appear to assume that the  $\delta p$  are orthogonal under the weighting function  $c^{-2}$  and that  $\int dz \rho_0 c^{-2} |\delta p|^2 \sim 1$ . Both of these are true for sound waves, the main focus of their paper. However, for IGWs,  $\int dz \rho_0 c^{-2} |\delta p|^2 \sim \mathcal{M}^2$ , and the  $\delta p$  are only orthogonal under the weighting function 1 (see Appendix C for further discussion on orthogonality).

Press also derives this result more rigorously using the method of variation of parameters, which is equivalent to using a Green’s function. In addition, Press considers the case in which  $N^2$  is continuous at the interface. He only treats this case in the limit in which  $\omega \sim N_0$ , and finds

$$\xi_z \sim \frac{1}{k}, \quad (\text{P81; eq. 88}) \quad (58)$$

the same result as eqn. 57. However, note that if  $\omega \sim N_0$ , then  $N_0 k_\perp d / \omega \ll 1$ , and the smooth result cannot be used (these waves see the interface as discontinuous). In addition, Press’s use of standard WKB matching to treat the smooth  $N^2$  profile is generally not applicable (see Appendix A).

Finally, we consider the work of B09. In their paper, Belkacem et al. numerically calculate the eigenfunctions for a solar structure model, use a convection simulation to specify the source term, and solve an amplitude equation in the same way as GK90. It is unclear whether the  $N^2$  profile in their solar structure model has a smooth transition between the radiative and convection zones—their  $N^2$  profile is discontinuous (Section 3.1) or has an abrupt transition (Appendix B), they will derive different eigenfunctions than for a smooth tanh profile (Appendix A). These eigenfunctions will produce a smaller flux (eqns. 41, B21) than we predict for a more realistic radiative-convective transition (eqn. 49).

Another key difference is that Belkacem et al. use an eddy-time correlation function  $\chi_k(\omega)$ , which in the notation of this paper can be written as  $\chi(\omega; \omega_e)$ . This function describes how efficiently an eddy with size  $1/k$  and turn-over frequency  $\omega_e = u_k k$  excites a wave with frequency  $\omega$ . Our analysis implicitly assumes  $\chi(\omega; \omega_e) \sim \exp(-\omega^2 / \omega_e^2)$ . This Gaussian eddy-time correlation function implies that eddies with turn-over frequencies  $\omega_e$  only excite waves with frequencies  $\omega$ . However, the turbulence in the convection simulation in B09 is not well described by a Gaussian eddy-time correlation function. Instead, Belkacem et al. find that a Lorentzian distribution,  $\chi(\omega; \omega_e) \sim (1 + 2(\omega / \omega_e)^2)^{-1}$ , is more accurate. This indicates that waves with frequency  $\omega$  can be excited by a broad range of eddies. In general, this makes wave excitation more efficient. It would be straightforward to generalize our results to this Lorentzian expression for  $\chi(\omega; \omega_e)$ .

## 6 DISCUSSION & CONCLUSIONS

In this paper we have calculated the excitation of internal gravity waves (IGW) by turbulent convection, motivated by the application to stellar convection. We assume that the source term exciting the IGWs can be modeled by Reynolds stresses associated with uncorrelated eddies in a Kolmogorov turbulent cascade. Our main results are the IGW fluxes, eqns. 41 & 49. In particular, we predict a *larger wave flux than previous calculations for low frequency waves* which satisfy  $N_0 k_\perp d / \omega \gg 1$ , where  $N_0$  is the buoyancy frequency in the radiative zone,  $k_\perp$  and  $\omega$  are the horizontal wavenumber and frequency of the IGW, respectively, and  $d$  is the thickness of the transition region between the radiative and convection zones. We also reconcile somewhat disparate claims in the literature by showing that different methods, such as pressure balance arguments and solving the inhomogeneous wave equation, predict the same IGW power spectrum when using the same assumptions (Section 4).

An IGW with frequency  $\omega$  sees the transition between the radiative and convection zones as discontinuous if  $N_0 k_\perp d / \omega \ll 1$ . In this case, the total flux is  $F^d \sim F_{\text{conv}} \mathcal{M}$ , as derived in past work, where  $F_{\text{conv}}$  is the convective flux and  $\mathcal{M}$  is the convective

Mach number. The most efficiently excited waves have frequencies  $\omega \sim \omega_c$ , the eddy turn-over frequency of the largest turbulent eddies, and  $k_\perp \sim H^{-1}$ , the inverse of the pressure scale height. These most efficiently excited waves are marginally susceptible to wave breaking when they enter the radiative region.

If, however, the transition between radiative and convective regions is smooth (i.e.,  $N_0 k_\perp d / \omega \gg 1$ ), the problem becomes more complicated. The IGW flux depends on the structure of the buoyancy frequency  $N^2(z)$  near the transition between the radiative and convective regions. We parameterize the transition using a tanh profile, which is a smooth transition that we believe is a physically reasonable model. The wave excitation is more efficient when  $N^2$  is smooth because the IGW eigenfunctions change amplitude rapidly near the interface (as originally discussed by P81). The total IGW flux is  $F^s \sim F_{\text{conv}}(d/H) \gg F^d$ . Again, the most efficiently excited waves have frequencies  $\omega \sim \omega_c$  and  $k_\perp \sim H^{-1}$ . However, these waves are extremely prone to wave breaking, as  $k_z \xi_z \gg 1$  in the radiative region (e.g., P81). These “waves” will thus break immediately when they enter the radiative region. We interpret these perturbations as a form of penetrative convection—they do not stay coherent long enough to be truly considered waves. The flux of IGWs that are marginally susceptible to wave breaking (i.e., have  $k_z \xi_z \sim 1$ ) is  $F \sim F_{\text{conv}} \mathcal{M}^{5/8} (d/H)^{3/8}$ . This is larger than the discontinuous  $N^2$  flux by  $(MH/d)^{-3/8}$ . The flux is dominated by waves with frequencies  $\omega \sim \omega_c$  and wave numbers  $k_\perp \sim H^{-1} (MH/d)^{1/8}$ .

In the Sun,  $\omega_c \sim 10^{-3} N_0$ , so  $\mathcal{M} \sim 10^{-3}$  (e.g., Brown et al. 2012), and  $d$  is estimated to be  $\sim 0.1H$  (Christensen-Dalsgaard et al. 2011). IGWs produced by the energy bearing eddies have  $N_0 k_\perp d / \omega \sim 10^2$ , and thus the transition region must be treated as smooth. This suggests that the IGW flux in the Sun is

$$F \sim F_{\text{conv}} \mathcal{M}^{5/8} \left( \frac{d}{H} \right)^{3/8} \sim 5 \times 10^{-3} F_{\text{conv}}, \quad (\text{Sun}) \quad (59)$$

about five times larger than the flux in the discontinuous  $N^2$  case. The flux is dominated by waves with frequencies  $\sim \omega_c$ , and  $k_\perp \sim 0.5H^{-1}$ .

The increase in wave flux due to a smooth radiative-convective interface is only for waves with  $N_0 k_\perp d / \omega \gg 1$ , i.e., for low frequency waves. For certain applications (e.g., helioseismology), the flux of low frequency waves is unimportant. In particular, low frequency  $g$ -modes in the Sun and massive stars are strongly damped by radiative diffusion and are unlikely to be seen at the surface. Thus, the increase in wave flux we predict for low frequency waves does not change the expected amplitudes of potentially observable  $g$ -modes in main sequence stars.

However, low frequency waves are important for the angular momentum transport, mixing, and/or mass loss due to IGWs excited by stellar convection. For example, a larger IGW flux may increase the predicted mass loss in the final stages of the life of a massive star (Quataert & Shiode 2012) and in Type Ia supernova progenitors (Piro 2011). This will be studied in detail in future work.

In order to make a more accurate prediction of the wave flux and spectrum, one would need to use a stellar structure model with a realistic radiative-convective interface and a better representation of the convective turbulence, as in B09. Our results highlight the importance of adequately resolving the smooth transition between the radiative and convective regions in such calculations (which is not necessarily the case in many stellar structure models). A discontinuous or abrupt transition will give a qualitatively different IGW flux than a smooth transition.

In this paper we only consider IGWs excited by the Reynolds stress associated with turbulent convective motions. However, if  $N^2$  is smooth, we find that the most efficiently excited modes are very susceptible to wave breaking. Wave breaking produces turbulence and can lead to additional IGW generation (Fritts 2009). Put another way, penetrative convection can itself generate IGWs. When  $N^2$  is smooth, the flux in modes which are unstable to breaking is a significant fraction of  $F_{\text{conv}}$ ; thus the breaking process has the potential to excite a non-negligible flux of IGWs.

Perhaps the most promising way to test the results of this paper is through comparison with direct numerical simulations of a radiative zone adjacent to a convection zone (e.g., Rogers & Glatzmaier 2005; Brun et al. 2011). Although such simulations typically require artificially high conduction in the radiative zone, and it is unclear how to best identify IGWs (Dintrans et al. 2005), this is probably the simplest system in which one can quantify the IGW flux generated by convection. We hope that analysis of such simulations can provide a quantitative test of the theory derived in this paper in the near future.

## ACKNOWLEDGMENTS

This material is based upon work supported by the National Science Foundation Graduate Research Fellowship under Grant No. DGE 1106400. DL acknowledges support from a Hertz Foundation Fellowship. This work was also partially supported by NASA HTP grant NNX11AJ37G, a Simons Investigator award from the Simons Foundation to EQ, the David and Lucile Packard Foundation, and the Thomas Alison Schneider Chair in Physics at UC Berkeley. We especially thank G. Vasil for helping solve for the eigenfunctions in Appendix A and A. Lieb for helping understand the differences between the mode projection and Green's function formalisms.

## APPENDIX A: TANH PROFILE EIGENFUNCTIONS

We will derive the eigenfunctions for the equation

$$\frac{\partial^2}{\partial z^2} \xi_z + \left( \frac{N^2(z)}{\omega^2} - 1 \right) k_{\perp}^2 \xi_z = 0, \quad (\text{A1})$$

where

$$N^2(z) = \frac{N_0^2 + \omega_c^2}{2} \left( \tanh\left(-\frac{z}{d}\right) + 1 \right) - \omega_c^2. \quad (\text{A2})$$

The transition between oscillatory behavior and exponential behavior (where  $N^2(z) = \omega^2$ ) is at  $z_t$  given by

$$\frac{\omega^2 + \omega_c^2}{N_0^2 + \omega_c^2} \sim \exp\left(-2\frac{z_t}{d}\right). \quad (\text{A3})$$

The eigenfunction in the radiative zone is well approximated by the WKB solution,

$$\begin{aligned} \xi_z = & B_1 (N_0 k_{\perp} / \omega)^{1/2} k_z(z)^{-1/2} \cos\left(\int dz k_z(z) + \pi/4\right) \\ & + B_2 (N_0 k_{\perp} / \omega)^{1/2} k_z(z)^{-1/2} \sin\left(\int dz k_z(z) + \pi/4\right), \end{aligned} \quad (\text{A4})$$

where we define the vertical wavenumber to be

$$k_z^2(z) = k_{\perp}^2 \left( N^2(z) / \omega^2 - 1 \right). \quad (\text{A5})$$

Near  $z_t$ , the WKB solution in the radiative region diverges. We wish to derive a new set of functions which closely approximate the eigenfunctions for  $z > z_t$ .

In many problems, the WKB solutions near a turning point

can be asymptotically matched onto Airy functions, which provide a connection between exponentially decaying and oscillatory WKB solutions. However, we cannot use this approach when  $k_{\perp} d < 1$ ; in this parameter regime  $k_z^2(z)$  cannot be well approximated as linear near  $z_t$ . Instead, we will show that when  $k_{\perp} d < 1$  the eigenfunctions can be well approximated in terms of Bessel functions. Furthermore, these Bessel function solutions are also a good approximation when  $k_{\perp} d \geq 1$ .

To show this, first note that if  $\exp(-2z/d) \ll 1$ , we can approximate

$$N^2(z) \approx (N_0^2 + \omega_c^2) \exp\left(-\frac{2z}{d}\right) - \omega_c^2. \quad (\text{A6})$$

The solutions to the wave equation (eqn. A1) for this approximate  $N^2(z)$  function are

$$\begin{aligned} \xi_z = & C_1 J_{\bar{\omega} k_{\perp} d / \omega} \left( k_{\perp} d \frac{\sqrt{N_0^2 + \omega_c^2}}{\omega} \exp\left(-\frac{z}{d}\right) \right) \\ & + C_2 Y_{\bar{\omega} k_{\perp} d / \omega} \left( k_{\perp} d \frac{\sqrt{N_0^2 + \omega_c^2}}{\omega} \exp\left(-\frac{z}{d}\right) \right), \end{aligned} \quad (\text{A7})$$

where  $J$  and  $Y$  are the Bessel functions of the first and second kind, respectively. We have also defined  $\bar{\omega}^2 = \omega^2 + \omega_c^2$ , where  $\bar{\omega}/\omega$  ranges between  $\sqrt{2}$  and 1. These approximate the solution for large positive  $z$ . We can asymptotically match the Bessel functions onto the WKB solution in the radiative zone (eqn. A4). We will make use of the following asymptotic forms for  $J$  and  $Y$ :

$$J_{\alpha}(x) \sim \frac{1}{\Gamma(\alpha + 1)} \left( \frac{x}{2} \right)^{\alpha}, \quad (\text{A8})$$

$$Y_{\alpha}(x) \sim -\frac{\Gamma(\alpha)}{\pi} \left( \frac{2}{x} \right)^{\alpha}, \quad (\text{A9})$$

provided that  $0 < x \ll \sqrt{\alpha + 1}$ , and

$$J_{\alpha}(x) \sim \sqrt{\frac{2}{\pi x}} \cos\left(x - \frac{\alpha\pi}{2} - \frac{\pi}{4}\right), \quad (\text{A10})$$

$$Y_{\alpha}(x) \sim \sqrt{\frac{2}{\pi x}} \sin\left(x - \frac{\alpha\pi}{2} - \frac{\pi}{4}\right), \quad (\text{A11})$$

provided that  $x \gg |\alpha^2 + 1/4|$ .

We must consider two regimes, depending on the size of  $k_{\perp} d$ . First consider  $k_{\perp} d \ll 1$ . We can use the asymptotic formula for large arguments provided that

$$k_{\perp} d \frac{\sqrt{N_0^2 + \omega_c^2}}{\omega} \exp\left(-\frac{z}{d}\right) \gg \frac{1}{4}. \quad (\text{A12})$$

This constraint can be satisfied simultaneously with  $\exp(-2z/d) \ll 1$ , implying that the asymptotic form of the Bessel functions are good approximations to the eigenfunctions. If we approximate  $k_z^2(z)$  as

$$k_z^2(z) \approx k_{\perp}^2 \frac{N_0^2 + \omega_c^2}{\omega^2} \exp\left(-\frac{2z}{d}\right), \quad (\text{A13})$$

we can approximate eqn. A7 by

$$\begin{aligned} \xi_z \approx & C_1 \sqrt{\frac{2}{\pi d}} \left( k_z^2(z) \right)^{-1/4} \cos\left(-d \left( k_z^2(z) \right)^{1/2} + \frac{\pi \bar{\omega} k_{\perp} d}{2\omega} + \frac{\pi}{4}\right) \\ & - C_2 \sqrt{\frac{2}{\pi d}} \left( k_z^2(z) \right)^{-1/4} \sin\left(-d \left( k_z^2(z) \right)^{1/2} + \frac{\pi \bar{\omega} k_{\perp} d}{2\omega} + \frac{\pi}{4}\right). \end{aligned} \quad (\text{A14})$$

This matches onto the WKB solution in the radiative region since  $k_{\perp}d$  is small. The amplitudes are

$$C_1 = B_1 \left( \frac{\pi N_0 k_{\perp} d}{2\omega} \right)^{1/2}, \quad (\text{A15})$$

$$C_2 = -B_2 \left( \frac{\pi N_0 k_{\perp} d}{2\omega} \right)^{1/2}. \quad (\text{A16})$$

Now assume  $k_{\perp}d \gg 1$ . In this case, the asymptotic form of the Bessel functions for small argument is only valid when  $\exp(-z/d) \gg 1$ , i.e., for positions where the Bessel functions themselves are not a good approximation to the eigenfunctions ( $N^2(z)$  cannot be simplified as in eqn. A6 if  $\exp(-z/d) \gg 1$ ). However, in this limit we can use the WKB approximation in the convective region, and connect the two WKB solutions with Airy functions. Thus, in the convective region, we have

$$\begin{aligned} \xi_z \sim & (B_1/2)(N_0 k_{\perp}/\omega)^{1/2} k_z(z)^{-1/2} \exp\left(-\int_{z_i}^z dz' |k_z(z')|\right) \\ & + B_2 (N_0 k_{\perp}/\omega)^{1/2} k_z(z)^{-1/2} \exp\left(+\int_{z_i}^z dz' |k_z(z')|\right). \end{aligned} \quad (\text{A17})$$

For  $z$  much larger than  $z_i$ , this becomes

$$\begin{aligned} \xi_z \sim & \frac{B_1}{2} \left( \frac{N_0}{\omega} \right)^{1/2} \left( \frac{e}{2} \right)^{\bar{\omega} k_{\perp} d / \omega} \exp(-(z - z_i) k_{\perp} \bar{\omega} / \omega) \\ & + B_2 \left( \frac{N_0}{\omega} \right)^{1/2} \left( \frac{2}{e} \right)^{\bar{\omega} k_{\perp} d / \omega} \exp(+ (z - z_i) k_{\perp} \bar{\omega} / \omega), \end{aligned} \quad (\text{A18})$$

For  $z$  much larger than  $z_i$ , the Bessel functions are a good approximation to the eigenfunction. In the limit of large  $z$ , the Bessel functions become

$$\begin{aligned} \xi_z \sim & C_1 \left( \frac{1}{e\pi k_{\perp} d} \right)^{1/2} \left( \frac{e\bar{\omega}}{2\omega} \right)^{\bar{\omega} k_{\perp} d / \omega + 1/2} \exp\left(-\frac{(z - z_i) k_{\perp} \bar{\omega}}{\omega}\right) \\ & - C_2 \left( \frac{4}{e\pi k_{\perp} d} \right)^{1/2} \left( \frac{2\bar{\omega}}{e\bar{\omega}} \right)^{\bar{\omega} k_{\perp} d / \omega + 1/2} \exp\left(+\frac{(z - z_i) k_{\perp} \bar{\omega}}{\omega}\right). \end{aligned} \quad (\text{A19})$$

Thus, the Bessel function solution matches onto the WKB solution in the convective region when

$$C_1 = B_1 \left( \frac{\pi N_0 k_{\perp} d}{2\omega} \right)^{1/2} \left( \frac{\omega}{\bar{\omega}} \right)^{\bar{\omega} k_{\perp} d / \omega + 1/2}, \quad (\text{A20})$$

$$C_2 = -B_2 \left( \frac{\pi N_0 k_{\perp} d}{2\omega} \right)^{1/2} \left( \frac{\bar{\omega}}{\omega} \right)^{\bar{\omega} k_{\perp} d / \omega + 1/2}. \quad (\text{A21})$$

Using eqns. A15, A16 & A20, A21, we can approximate  $\xi_z$  by

$$\begin{aligned} \xi_z \sim & B_1 \left( \frac{\pi N_0 k_{\perp} d}{2\omega} \right)^{1/2} \left( \frac{\omega}{\bar{\omega}} \right)^{\bar{d}} J_{\bar{d}} \left[ k_{\perp} d \frac{\sqrt{N_0^2 + \omega_c^2}}{\omega} \exp\left(-\frac{z}{d}\right) \right] \\ & + B_2 \left( \frac{\pi N_0 k_{\perp} d}{2\omega} \right)^{1/2} \left( \frac{\bar{\omega}}{\omega} \right)^{\bar{d}} Y_{\bar{d}} \left[ k_{\perp} d \frac{\sqrt{N_0^2 + \omega_c^2}}{\omega} \exp\left(-\frac{z}{d}\right) \right], \end{aligned} \quad (\text{A22})$$

where we have defined  $\bar{d} = \bar{\omega} k_{\perp} d / \omega$ . This will be a good approximation for  $\xi_z(z)$  as long as  $\exp(-z/d) \ll 1$ .

For the purposes of determining the convective excitation of IGWs, we are interested in evaluating  $\xi_z$  between  $z_i$  and  $z_i + 1/k_{\perp}$ , where  $z_i$  is the location of the interface between the radiative and convective regions. Since

$$\frac{\omega_c^2}{N_0^2 + \omega_c^2} \sim \exp\left(-2\frac{z_i}{d}\right), \quad (\text{A23})$$

the argument of the Bessel functions varies from  $\omega_c k_{\perp} d / \omega$  to

$\exp(-(k_{\perp}d)^{-1})\omega_c k_{\perp} d / \omega$ . Within this range, the Bessel functions change by about a factor of  $e$ . It is thus within the accuracy of our calculation to take  $\xi_z$  to be about constant within this range: at  $z = z_i$ , we have that

$$\begin{aligned} \xi_z \sim & B_1 \left( \frac{\pi N_0 k_{\perp} d}{2\omega} \right)^{1/2} \left( \frac{\omega}{\bar{\omega}} \right)^{\bar{\omega} k_{\perp} d / \omega} J_{\bar{\omega} k_{\perp} d / \omega}(\omega_c k_{\perp} d / \omega) \\ & + B_2 \left( \frac{\pi N_0 k_{\perp} d}{2\omega} \right)^{1/2} \left( \frac{\bar{\omega}}{\omega} \right)^{\bar{\omega} k_{\perp} d / \omega} Y_{\bar{\omega} k_{\perp} d / \omega}(\omega_c k_{\perp} d / \omega). \end{aligned} \quad (\text{A24})$$

In evaluating eqn. A24, we need to calculate  $J_x(xa)$ , where  $x = \bar{\omega} k_{\perp} d / \omega$ , and  $a = \omega_c / \bar{\omega} < 1/\sqrt{2}$ . A good set of approximations for the Bessel functions for  $x \ll 1$  and  $x \gg 1$  is given in eqn. 22 of the main text (based on expansions of  $J_x(xa)$  from Abramowitz & Stegun (1972)).

## A1 Numerical Verification

Here we will present numerical verification of our approximate solutions in the above subsection. We numerically integrated the homogeneous differential equation (eqn. A1) with  $N^2$  given by eqn. A2 in Mathematica using the ‘‘ImplicitRungeKutta’’ method, and solved for a physical solution, satisfying  $\xi_z \rightarrow 0$  as  $z \rightarrow \infty$ . We pick the right boundary to be a point  $b$  deep within the convective region, where  $k_z^2(b) = -k_{\perp}^2$ , specify  $\xi_z(b) = 1$ ,  $\xi'_z(b) = -k_{\perp}$ , and integrate  $\xi_z$  leftwards into the radiative region. This ensures that  $\xi_z$  satisfies the boundary condition  $z \rightarrow +\infty$ . We find that our calculations are insensitive to the value of  $b$ , provided that it is sufficiently larger than  $z_i$ .

To test the approximations described in the above subsection, we calculate the value of the physical eigenfunction at the interface between the radiative and convective regions  $\xi_z(z_i)$ . Because any multiple of the eigenfunction is also an eigenfunction, we normalize by  $B_1$  (see eqn. A4), which is the amplitude of the oscillations deep in the radiative zone. Equation A24 predicts

$$\xi_z(z_i)/B_1 = \left( \frac{\pi N_0 k_{\perp} d}{2\omega} \right)^{1/2} \left( \frac{\omega}{\bar{\omega}} \right)^{\bar{\omega} k_{\perp} d / \omega} J_{\bar{\omega} k_{\perp} d / \omega} \left( k_{\perp} d \frac{\omega_c}{\omega} \right). \quad (\text{A25})$$

Our analysis is only valid if we are in the smooth  $N^2$  limit, i.e., if  $N_0 k_{\perp} d / \omega \gg 1$ .

In Figure A1 we compare our numerical results to the analytic predictions. In Figure A1 (top panel) we vary  $\omega/N_0$  for two different values of  $k_{\perp}d$ . The numerical solutions agree with our prediction when  $N_0 k_{\perp} d / \omega \gg 1$ . In the opposite limit, when  $N_0 k_{\perp} d / \omega \ll 1$ , we can treat  $N^2$  as discontinuous, so  $\xi_z$  is continuous across the interface, and  $\xi_z(z_i)/B_1 = 1$ , as is the case for the lower curve in Figure A1 (top panel). In Figure A1 (bottom panel) we vary  $k_{\perp}d$ , fixing  $\omega/N_0 = 0.01$ , for two values of  $\omega_c/N_0$ . In this case, we have  $N_0 k_{\perp} d / \omega = 1$  when  $k_{\perp}d = 0.01$ . The normalized eigenfunctions approach one as  $k_{\perp}d$  decreases, and the numerical solutions begin to deviate slightly from the analytic prediction near  $k_{\perp}d = 0.01$ . These results indicate that our analytic solution for  $\xi_z$  near  $z_i$  is accurate provided we are in the smooth  $N^2$  limit. The numerical solutions also show how the eigenfunctions transition between the smooth and discontinuous  $N^2$  limits.

## APPENDIX B: PIECEWISE LINEAR $N^2$

In the limit of smooth  $N^2$ , the eigenfunctions, Green’s function, and IGW flux all depend on the nature of the transition between radiative and convective regions. In this paper, we focus on the case of a

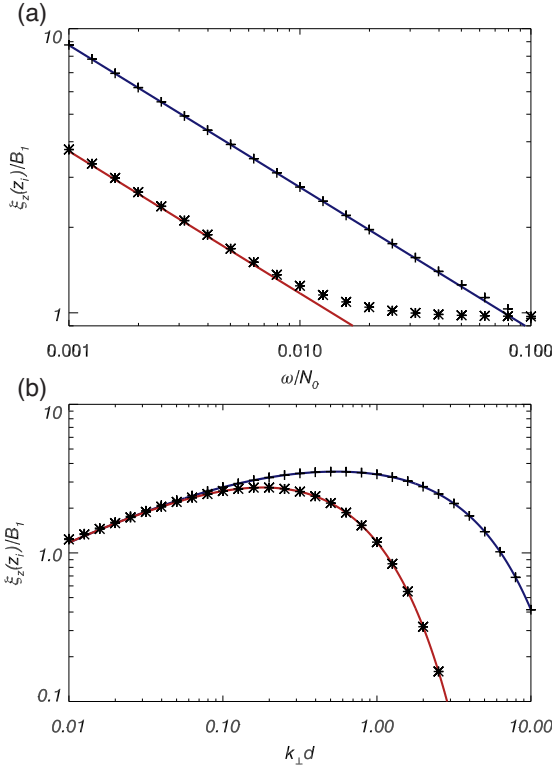


**Figure A1.** The normalized eigenfunction at the radiative-convective interface  $z_i$ . The symbols denote the numerical solution, and the lines denote the analytic prediction, eqn. A24. In the top panel, we vary  $\omega/N_0$ , fixing  $\omega_c = \omega$ . The blue line and crosses have  $k_\perp d = 0.1$ , and the red line and asterisks have  $k_\perp d = 0.01$ . The numerical solution matches the analytic prediction for smooth  $N^2$  when  $N_0 k_\perp d / \omega \gg 1$ , and approaches one (the discontinuous  $N^2$  solution) when  $N_0 k_\perp d / \omega \ll 1$ . In the bottom panel, we vary  $k_\perp d$ , fixing  $\omega/N_0 = 0.01$  and setting  $\omega_c/N_0 = 0.01$  (blue curve, crosses) or  $\omega_c/N_0 = 0.002$  (red curve, asterisks). Again, there is good agreement between the numerical solution and the analytic prediction.

tanh profile (Appendix A), as we think it is the best simple model of this transition region. However, in this appendix, we consider another analytically tractable transition—a piecewise linear  $N^2$  profile. This is the most abrupt transition possible, and thus not very physical. However, we find it instructive to consider a second example of a transition to explicitly demonstrate that the results depend on the details of the transition region. In particular, this highlights that care must be taken to use a smooth  $N^2$  profile when numerically solving for wave excitation using a stellar structure model (as in, e.g., B09).

We assume  $N^2$  is given by

$$N^2(z) = \begin{cases} N_0^2 & \text{if } z \leq -d/2, \\ (N_0^2 - \omega_c^2)/2 - (N_0^2 + \omega_c^2)(z/d) & \text{if } -d/2 < z < d/2, \\ -\omega_c^2 & \text{if } z \geq d/2. \end{cases} \quad (\text{B1})$$

We have that  $N^2(z) = \omega^2$  at the point

$$z_t = \frac{N_0^2 - 2\omega^2 - \omega_c^2}{N_0^2 + \omega_c^2} \left( \frac{d}{2} \right), \quad (\text{B2})$$

and that  $N^2(z) = 0$  at

$$z_i = \frac{N_0^2 - \omega_c^2}{N_0^2 + \omega_c^2} \left( \frac{d}{2} \right). \quad (\text{B3})$$

The solutions in each region are

$$\xi_z = B_1 \cos(N_0 k_\perp (z + d/2)/\omega) + B_2 \sin(N_0 k_\perp (z + d/2)/\omega), \quad (\text{B4})$$

for  $z < -d/2$ ,

$$\xi_z = C_1 \exp(-k_\perp (z - d/2)) + C_2 \exp(k_\perp (z - d/2)), \quad (\text{B5})$$

for  $z > d/2$ ,

$$\xi_z = D_1 \text{Ai}(K_1^{1/3}(z - z_t)) + D_2 \text{Bi}(K_1^{1/3}(z - z_t)), \quad (\text{B6})$$

for  $-d/2 < z < d/2$ ,

where Ai, Bi are the Airy functions of the first and second kind, and

$$K_1 = \frac{dk_z^2(z)}{dz} \Big|_{z_i} = \frac{k_\perp^2 N_0^2 + \omega_c^2}{d \omega^2}. \quad (\text{B7})$$

We can relate the six coefficients in eqns. B4–B6 to one another using four boundary conditions:  $\xi_z$  and  $\xi'_z$  must be continuous at  $z = \pm d/2$ .

First consider the boundary at  $z = +d/2$ . The argument of the Airy functions at this boundary is

$$(k_\perp d)^{2/3} \left( \frac{\omega^2 + \omega_c^2}{(N_0^2 + \omega_c^2)^{2/3} (\omega^2)^{1/3}} \right) \sim \left( \frac{\omega^2 k_\perp d}{N_0^2} \right)^{2/3}. \quad (\text{B8})$$

This is much smaller than one unless  $k_\perp d$  is extremely large. One can check that IGW excitation is exponentially suppressed when  $\omega^2 k_\perp d / N_0^2 \gg 1$ . Thus, we will assume that  $\omega^2 k_\perp d / N_0^2 \ll 1$ . This implies that  $\text{Ai}|_{d/2}, \text{Bi}|_{d/2}, \text{Ai}'|_{d/2}, \text{Bi}'|_{d/2}$  are all of order one, where we have introduced the shorthand  $\text{Ai}|_z = \text{Ai}(K_1^{1/3}(z - z_t))$ , and similarly for the other functions. To order of magnitude, we have that

$$C_1 + C_2 \sim D_1 \text{Ai}|_{d/2} + D_2 \text{Bi}|_{d/2}, \quad (\text{B9})$$

and

$$C_1 - C_2 \sim \frac{K_1^{1/3}}{k_\perp} (D_1 \text{Ai}'|_{d/2} + D_2 \text{Bi}'|_{d/2}). \quad (\text{B10})$$

Notice that

$$K_1^{1/3}/k_\perp \sim \left( \frac{1}{k_\perp d} \frac{N_0^2 + \omega_c^2}{\omega^2} \right)^{1/3} \gg 1. \quad (\text{B11})$$

Now consider the boundary at  $z = -d/2$ . The argument of the Airy functions at this boundary is

$$(k_\perp d)^{2/3} \left( \frac{N_0^2 + \omega_c^2}{\omega^2} \right)^{1/3} \sim \left( \frac{N_0 k_\perp d}{\omega} \right)^{2/3} \gg 1, \quad (\text{B12})$$

where the last inequality follows from assuming that we are in the smooth  $N^2$  limit. We thus have

$$\xi_z|_{-d/2} \sim \left( \frac{N_0 k_\perp d}{\omega} \right)^{-1/6} \times \left[ D_1 \cos\left( \frac{2}{3} \frac{N_0 k_\perp d}{\omega} + \frac{\pi}{4} \right) + D_2 \sin\left( \frac{2}{3} \frac{N_0 k_\perp d}{\omega} + \frac{\pi}{4} \right) \right], \quad (\text{B13})$$

implying

$$B_1 \sim \left( \frac{N_0 k_\perp d}{\omega} \right)^{-1/6} (D_1 \cos(\phi) + D_2 \sin(\phi)), \quad (\text{B14})$$

where  $\phi = (2/3)(N_0 k_\perp d / \omega) + \pi/4$ . Similarly, by comparing  $\xi'_z$  on either side of  $z = -d/2$  we find

$$B_2 \sim \left( \frac{N_0 k_\perp d}{\omega} \right)^{-1/6} (-D_1 \sin(\phi) + D_2 \cos(\phi)). \quad (\text{B15})$$

Using these boundary conditions, we find that the physical eigenfunction is

$$\eta_z^l \sim \begin{cases} B_1 \cos\left(\frac{N_0 k_\perp (z+d/2)}{\omega}\right) + B_2 \sin\left(\frac{N_0 k_\perp (z+d/2)}{\omega}\right) & z < -d/2, \\ \tilde{B}_1 \left(\frac{N_0 k_\perp d}{\omega}\right)^{1/6} \exp(-k_\perp (z-d/2)) & z > d/2, \end{cases} \quad (\text{B16})$$

where we use *superscript l* to denote the eigenfunction for the *piecewise linear*  $N^2$  profile, and  $\tilde{B}_1 \sim B_2 \sim B_1$ . An unphysical eigenfunction is

$$\xi_z^l \sim \begin{cases} B_2 \sin\left(\frac{N_0 k_\perp (z+d/2)}{\omega}\right) & z < -d/2, \\ \left(\frac{N_0 k_\perp d}{\omega}\right)^{-1/6} \frac{N_0}{\omega} \times \\ \left(\tilde{B}_1 \exp(-k_\perp (z-d/2)) + \tilde{B}_2 \exp(k_\perp (z-d/2))\right) & z > d/2, \end{cases} \quad (\text{B17})$$

where  $\tilde{B}_2 \sim \tilde{B}_1 \sim B_2$ . Note that the constants  $B_1, B_2$  in  $\eta_z^l$  and  $\tilde{B}_1, \tilde{B}_2$  in  $\xi_z^l$  vary sinusoidally with  $d$  (as well as the other parameters of the problem). Thus, although for most values of  $d$  they are the same size, there are specific values of  $d$  for which one term is much larger than the other.

The Green's function for  $z < 0$  and  $\zeta > 0$  is then

$$G^l(z, t, \zeta, \tau) \sim \sum_{\omega'} \frac{\omega' \sqrt{\rho_0}}{N_0 k_\perp \sqrt{L}} \left(\frac{N_0 k_\perp d}{\omega'}\right)^{1/6} \times \xi_z^l(z; \omega') \exp(-k_\perp \zeta - i\omega'(t - \tau)). \quad (\text{B18})$$

This implies that the IGW flux is

$$\frac{dF^l}{d \log \omega \, d \log k_\perp} \sim \rho_0 u_c^3 \mathcal{M}^{2/3} (k_\perp H)^4 \left(\frac{\omega}{\omega_c}\right)^{-41/6} (k_\perp d)^{1/3}, \quad (\text{B19})$$

assuming  $\omega \gtrsim \omega_c$ ,  $k_\perp \lesssim k_\perp^{\max}(\omega) \sim H^{-1}(\omega/\omega_c)^{3/2}$ , and  $k_\perp \ll d^{-1}(N_0/\omega)^2$ . The typical rms vertical displacement satisfies

$$k_z \xi_z \sim \mathcal{M}^{-1/6} (k_\perp H)^{11/3} \left(\frac{\omega}{\omega_c}\right)^{-65/12} \left(\frac{d}{H}\right)^{1/6} \quad (\text{B20})$$

We find that the most efficiently excited waves are susceptible to wave breaking. The flux of waves marginally susceptible to wave breaking is

$$F^l \sim F_{\text{conv}} \mathcal{M} \left(\frac{d}{\mathcal{M}H}\right)^{3/22}. \quad (\text{B21})$$

Using  $\mathcal{M} \sim 10^{-3}$  and  $d = 0.1H$  (Section 6), we find  $F^l \sim 1.87F_{\text{conv}}\mathcal{M}$ . This is a very modest increase over the discontinuous IGW flux (see Section 3.5).

### APPENDIX C: MODE PROJECTION FORMALISM (GK90)

In GK90, an amplitude equation is derived by projecting the inhomogeneous wave equation onto specific modes. We will show that their approach gives the same result as our Green's function approach, provided that the correct inner product is used.

First start with the inhomogeneous equation for  $\xi_z$  in the Boussinesq approximation

$$\nabla^2 \frac{\partial^2}{\partial t^2} \xi_z + N^2 \nabla_\perp^2 \xi_z = S. \quad (\text{C1})$$

In the mode projection formalism, we decompose  $\xi_z$  as

$$\xi_z = \frac{1}{\sqrt{\mathcal{A}}} \sum_{\omega'} A(t; \omega') \eta_z(z; \omega') \exp(ik_x x + ik_y y - i\omega' t), \quad (\text{C2})$$

where  $\eta_z(z; \omega')$  are the physical solutions satisfying the homogeneous wave equation. Substituting this into the inhomogeneous wave equation, multiplying by  $\rho_0 \eta_z^*(z; \omega) \exp(-ik_x x - ik_y y + i\omega t)$  and integrating over  $d^3 x dt$ , we find

$$|A(t; \omega)| = \frac{\omega}{2k_\perp^2 \sqrt{\mathcal{A}}} \int_{-\infty}^t d\tau \int dxdy \exp(-ik_x x - ik_y y + i\omega\tau) \times \int_{z_i}^L d\zeta \rho_0 S(x, y, \zeta, \tau) \eta_z^*(\zeta; \omega). \quad (\text{C3})$$

A crucial step in deriving this is using

$$\int dz \rho_0 \partial_z \eta_z(z; \omega') \partial_z \eta_z^*(z; \omega) = \delta_{\omega\omega'} \frac{k_\perp^2}{\omega\omega'}. \quad (\text{C4})$$

That is, the  $\eta_z(z; \omega)$  are orthogonal with respect to the inner product  $\langle a, b \rangle = \int dz \rho_0 \partial_z a \partial_z b^*$ . This follows from our normalization equation (eqn. 26) and the polarization conditions (eqn. 6).

Although we use  $\xi_z$  as our perturbation variable in this paper, GK90 uses  $\delta p$ . The inhomogeneous wave equation for  $\delta p$  in the Boussinesq approximation is

$$\nabla^2 \frac{\partial^2}{\partial t^2} \delta p + N^2 \nabla_\perp^2 \delta p = \bar{S}, \quad (\text{C5})$$

where  $\bar{S} \sim (\rho_0 \omega^2 / k_\perp) S$ . As above, we can decompose  $\delta p$  into eigenmodes

$$\delta p = \frac{1}{\sqrt{\mathcal{A}}} \sum_{\omega'} A(t; \omega') \delta p(z; \omega') \exp(ik_x x + ik_y y - i\omega' t), \quad (\text{C6})$$

where  $\delta p(z; \omega')$  are the physical solutions satisfying the homogeneous wave equation. When we put this into the inhomogeneous wave equation, multiply by  $\rho_0 \delta p^*(z; \omega) \exp(-ik_x x - ik_y y + i\omega t)$ , and integrate over  $d^3 x dt$ , one might think that

$$|A(t; \omega)| \stackrel{?}{=} \int_{-\infty}^t d\tau \int dxdy \exp(-ik_x x - ik_y y + i\omega\tau) \times \frac{1}{2\omega N_0^2 \rho_0^2 \sqrt{\mathcal{A}}} \int_{z_i}^L d\zeta \rho_0 \bar{S}(x, y, \zeta, \tau) \delta p^*(\zeta; \omega). \quad (\text{C7})$$

Using  $\delta p(\zeta; \omega) \sim (\rho_0 \omega^2 / k_\perp) \eta_z(\zeta; \omega)$  (eqn. 9), we see that this estimate of  $|A(t; \omega)|$  differs from our estimate using  $\xi_z$  (eqn. C3) by  $\omega^2 / N_0^2$ . This leads to an underestimation of the flux in IGWs by  $\sim \mathcal{M}^4$ .

The discrepancy is due to using the incorrect inner product. Implicit in the derivation of eqn. C7 is the assumption that the  $\delta p$  are orthogonal under the same inner product as the  $\xi_z$ , i.e.,

$$\int dz \rho_0 \partial_z \delta p(z; \omega') \partial_z \delta p^*(z; \omega) \stackrel{?}{=} \delta_{\omega\omega'} \rho_0^2 N_0^2. \quad (\text{C8})$$

However, one can check that the  $\delta p$  are not orthogonal with respect to this inner product.<sup>3</sup> Rather, they are orthogonal with respect to  $\langle a, b \rangle = \int dz \rho_0^{-1} a b^*$ , i.e.,

$$\int dz \rho_0^{-1} \delta p(z; \omega') \delta p^*(z; \omega) = \delta_{\omega\omega'} \frac{\omega^2}{k_\perp^2}. \quad (\text{C9})$$

<sup>3</sup> Using the properties of Hermitian operators, one can show that the  $\delta p$  IGW eigenfunctions of eqn. C5 are orthogonal under the inner product defined in eqn. C8. However, for the mode projection to be well defined, we must work in a complete basis, and the IGWs alone do not form a complete basis (in the convection zone). Our resolution of this apparent inconsistency is to note that the eigenfunctions of the full non-Boussinesq wave equation *do* form a complete basis (this includes sound waves in addition to IGWs). Moreover, one can show that the  $\delta p$  eigenfunctions for the non-Boussinesq equations are only orthogonal under the inner product defined in eqn. C9.

Thus, if we integrate the inhomogeneous wave equation twice with respect to  $z$ , multiply by  $\rho_0^{-1}\delta p^*(z; \omega) \exp(-ik_x x - ik_y y + i\omega t)$ , and integrate over  $d^3 x dt$ , we get

$$|A(t; \omega)| = \frac{1}{2\omega^3 \sqrt{\mathcal{A}}} \int_{-\infty}^t d\tau \int dxdy \exp(-ik_x x - ik_y y + i\omega t) \times \int_{z_i}^L d\zeta \rho_0^{-1} \bar{S}(x, y, \zeta, \tau) \delta p^*(\zeta; \omega). \quad (\text{C10})$$

One can check that this is consistent with the calculation using  $\xi_z$ .

If one uses a Green's function this issue of orthogonality under different inner products becomes trivial. Using the expansions in Sec. 3.3, we have

$$\frac{1}{\sqrt{\mathcal{A}}} \sum_{\omega'} A(t; \omega') \xi_{z,\text{rad}}(z; \omega') \exp(ik_x x + ik_y y - i\omega' t) = \int_{-\infty}^t d\tau \int_{z_i}^L d\zeta \sum_{\omega'} \frac{\xi_{z,\text{rad}}(z; \omega') \eta_z(\zeta; \omega')}{N_0 k_{\perp} L W(\zeta)} S \exp(-i\omega'(t - \tau)), \quad (\text{C11})$$

where  $z < z_i$ . Since both the left and right hand sides are in the span of  $\{\xi_{z,\text{rad}}\}_{\omega}$ , we can simply use the inner product defined by

$$\langle \xi_{z,\text{rad}}(z; \omega), \xi_{z,\text{rad}}(z; \omega') \rangle = \delta_{\omega\omega'}. \quad (\text{C12})$$

Taking  $\langle \xi_{z,\text{rad}}(z; \omega), \cdot \rangle$  of eqn. C11, multiplying by  $\exp(-ik_x x - ik_y y + i\omega t)$ , and integrating in the horizontal directions, we get

$$A(t; \omega) = \frac{1}{\sqrt{\mathcal{A}}} \int_{-\infty}^t d\tau \int dxdy \int_{z_i}^L d\zeta \frac{1}{N_0 k_{\perp} L} \frac{\eta_z(\zeta; \omega)}{W(\zeta)} \times S(x, y, \zeta, \tau) \exp(-ik_x x - ik_y y + i\omega\tau). \quad (\text{C13})$$

This is eqn. 24, which can easily be manipulated into eqns. 28, 29 using the eigenfunctions. Note that we cannot use such an inner product in the mode decomposition formalism because we need to calculate terms like  $\langle \delta p^*(\zeta; \omega), S(x, y, \zeta, \tau) \rangle$ , and thus need an explicit formula for the inner product in terms of integrals over  $\zeta$ .

Finally, we will demonstrate that the mode projection formalism—when done correctly—and the Green's function formalism give the same result. Specifically, we will show that eqns. C3 and C13 are equivalent. First note that  $W(\zeta)$  is a constant for our wave equation. We want to show that

$$\frac{1}{N_0 k_{\perp} L W} = \frac{\rho_0 \omega}{2k_{\perp}^2}. \quad (\text{C14})$$

We can evaluate  $W$  in the radiative zone, and find

$$W = \frac{2N_0 k_{\perp} B_1 B_2}{\omega} \sim \frac{2k_{\perp}}{N_0 \omega L \rho_0}, \quad (\text{C15})$$

where we have used eqn. 27. This proves that the two formulations are equivalent.

## REFERENCES

- Abramowitz M., Stegun I. A., 1972, Handbook of Mathematical Functions  
 Baldwin M. P. et al., 2001, Reviews of Geophysics, 39, 179  
 Brookes J. R., Isaak G. R., van der Raay H. B., 1976, Nature, 259, 92  
 Brown B. P., Vasil G. M., Zweibel E. G., 2012, ApJ, 756, 109  
 Brun A. S., Miesch M. S., Toomre J., 2011, ApJ, 742, 79  
 Charbonnel C., Talon S., 2005, Science, 309, 2189  
 Christensen-Dalsgaard J., Monteiro M. J. P. F. G., Rempel M., Thompson M. J., 2011, MNRAS, 414, 1158

- Dintrans B., Brandenburg A., Nordlund Å., Stein R. F., 2005, A&A, 438, 365  
 Fritts D. C., Alexander M. J., 2003, Reviews of Geophysics, 41, 1003  
 Garcia Lopez R. J., Spruit H. C., 1991, ApJ, 377, 268  
 Goldreich P., Keeley D. A., 1977, ApJ, 212, 243  
 Goldreich P., Kumar P., 1990, ApJ, 363, 694  
 Kumar P., Quataert E. J., 1997, ApJL, 475, L143  
 Meakin C. A., Arnett D., 2007, ApJ, 667, 448  
 Piro A. L., 2011, ApJL, 738, L5  
 Press W. H., 1981, ApJ, 245, 286  
 Quataert E., Shiode J., 2012, MNRAS, 423, L92  
 Rogers T. M., Glatzmaier G. A., 2005, MNRAS, 364, 1135  
 Rogers T. M., Lin D. N. C., Lau H. H. B., 2012, ApJL, 758, L6  
 Severnyi A. B., Kotov V. A., Tsap T. T., 1976, Nature, 259, 87  
 Talon S., Charbonnel C., 1998, A&A, 335, 959  
 Talon S., Kumar P., Zahn J.-P., 2002, ApJL, 574, L175  
 Turck-Chièze S. et al., 2001, ApJL, 555, L69  
 Unno W., Osaki Y., Ando H., Saio H., Shibahashi H., 1989, Non-radial oscillations of stars  
 Zahn J.-P., Talon S., Matias J., 1997, A&A, 322, 320